

Monte-Carlo statistical hadronization in relativistic heavy-ion collisions

Radoslaw Ryblewski

Abstract A brief introduction to the statistical hadronization approach to particle production in relativistic heavy-ion collisions is given. In the context of fluid dynamics modeling various aspects of hadron emission at the freeze-out are discussed. Practical applications of the presented concepts are presented within the THERMINATOR Monte-Carlo hadron generator.

1 Relativistic heavy-ion collisions

The relativistic heavy-ion collision experiments are a perfect tool for studying, in a controlled and reproducible manner, the properties of strongly interacting matter at high energies. Unlike the collisions of more elementary particles, they provide unique opportunity to reach the thermodynamic equilibrium needed for investigating the phase diagram and transport properties of the QCD matter. Assuming that (local) thermal equilibrium is achieved promptly, and that the interactions are strong enough to maintain this state throughout subsequent evolution, the expansion of such a system should, in principle, follow the laws of relativistic fluid dynamics [1]¹. Given initial conditions for initialization of fluid dynamical fields, and the prescription for the hadron emission from the fluid, the fluid dynamics provides straightforward and intuitive way to study properties of the produced matter, as encoded in its equation of state. Although still some important questions remain, *e.g.*, concerning the formulation of the theory itself [11] (in particular related to the form of the transport coefficients [12, 13, 14]), the successes of the models employing fluid dynamics concepts already have shown (almost)-perfect fluidity of the quark-

Radoslaw Ryblewski
Institute of Nuclear Physics, Polish Academy of Sciences, PL-31342 Kraków, Poland,
e-mail: Radoslaw.Ryblewski@ifj.edu.pl

¹ Note that several recent studies indicate that fluid dynamics may be applicable also in the situations where the produced system is locally far off equilibrium [2, 3, 4, 5, 6], see also [7, 8, 9, 10].

gluon plasma and established a sort of hydro-like “Standard Model” of heavy-ion collisions. While recently a significant progress in the determination of the initial state of heavy-ion collisions has been made, using, *i.a.*, non-equilibrium effective field theory and gauge/gravity correspondence, the hadronic production from such a system is still poorly understood. Huge majority of the approaches use (to some level heuristic, yet surprisingly successful) prescriptions for the hadronization process dating back to times of Fermi, Landau, and Hagedorn.

In these lectures we will briefly review some of the concepts of particle decoupling and statistical hadronization as applied to heavy-ion collisions showing, in the end, their remarkable efficacy in describing some of experimentally observed phenomena.

In this work we use natural units where $c = k_B = \hbar = 1$. The bold font denotes the vectors in the transverse $x - y$ plane.

2 Relativistic perfect fluid dynamics

The simplest and, at the same time, the only unambiguously ² derivable relativistic fluid dynamical equations are that of *relativistic perfect fluid dynamics* [16, 17, 18, 19]. Due to their simplicity they are extensively applied to various systems in physics, including the evolution of strongly interacting matter produced in relativistic heavy-ion collisions. Although the literature on the subject is rather extensive (see *i.e.* Refs. [11, 20, 21, 22, 23, 24, 25, 26, 27] and the references therein), we will review herein its basic aspects to set the stage for further discussion.

The equations of relativistic perfect fluid dynamics for the (net) charge-free matter follow solely from the local conservation laws of energy and momentum [16, 17, 18, 19], which in the Minkowski coordinates may be formulated in the following covariant form ³

$$\partial_\mu T^{\mu\nu}(x) = 0, \quad (1)$$

where $T^{\mu\nu}(x)$ is the energy-momentum tensor and $x^\mu = (t, \mathbf{x}_T, z)$.

In addition, for a multicomponent system which possesses N conserved charges Q_i one should supplement Eq. (1) with N continuity equations for the respective charge currents N_i^μ

$$\partial_\mu N_i^\mu(x) = 0 \quad (i = 1 \dots N). \quad (2)$$

² Some sort of ambiguity arises in the case when dissipative effects are present in the system. In such a situation additional assumptions on the evolution of dissipative quantities (*e.g.* shear stress tensor and bulk viscous pressure) are required, resulting in additional equations of motion. The latter may differ significantly in various approaches [15].

³ In the case of curvilinear coordinates, even if the space-time is considered to be flat (in the sense of globally vanishing Riemann tensor), one should replace the partial derivative $\partial_\mu = (\partial_t, -\nabla)$ in Eq. (1) with *covariant derivative* d_μ .

One may consider, *i.e.*, $Q_i = \{B, I_3, S, C\}$, where B, I_3, S and C denote baryon number, third component of the isospin, strangeness and charm, respectively⁴.

The main assumption defining the perfect fluid is that each fluid element, when considered in its local rest frame (LRF), is exactly in *thermal and chemical equilibrium* state. This is expressed by the static equilibrium (isotropic) form of the energy-momentum tensor

$$T_{\text{LRF}}^{\mu\nu}(x) = \text{diag} \left(\mathcal{E}(x), \mathcal{P}(x), \mathcal{P}(x), \mathcal{P}(x) \right), \quad (3)$$

where $\mathcal{E}(x)$ and $\mathcal{P}(x)$ denote the equilibrium energy density and pressure, respectively. One may also easily convince oneself that in the perfect fluid case the charge currents must all have the following LRF form

$$N_{i,\text{LRF}}^{\mu}(x) = \left(\mathcal{N}_i(x), 0, 0, 0 \right), \quad (4)$$

where $\mathcal{N}_i(x)$ represents the density of the charge Q_i ; otherwise dissipative effects have to occur.

In general (laboratory) frame each fluid element moves with a fluid four-velocity $u^{\mu}(x) \equiv \gamma(1, \mathbf{v}_T, v_z)$, satisfying normalization condition $u^{\mu}u_{\mu} = 1$. The form of the energy-momentum tensor in this frame can be obtained by applying a general (canonical) Lorentz boost transformation to Eq. (3)

$$T^{\mu\nu}(x) = \Lambda_{\alpha}^{\mu}(u^{\lambda}) \Lambda_{\beta}^{\nu}(u^{\lambda}) T_{\text{LRF}}^{\alpha\beta}(x), \quad (5)$$

where the boost matrix Λ_{ν}^{μ} is defined as follows

$$\Lambda_{\nu}^{\mu}(u^{\lambda}) \equiv \begin{pmatrix} \gamma & -\gamma v_x & -\gamma v_y & -\gamma v_z \\ -\gamma v_x & 1 + (\gamma - 1) \frac{v_x^2}{v^2} & (\gamma - 1) \frac{v_x v_y}{v^2} & (\gamma - 1) \frac{v_x v_z}{v^2} \\ -\gamma v_y & (\gamma - 1) \frac{v_x v_y}{v^2} & 1 + (\gamma - 1) \frac{v_y^2}{v^2} & (\gamma - 1) \frac{v_y v_z}{v^2} \\ -\gamma v_z & (\gamma - 1) \frac{v_x v_z}{v^2} & (\gamma - 1) \frac{v_y v_z}{v^2} & 1 + (\gamma - 1) \frac{v_z^2}{v^2} \end{pmatrix}. \quad (6)$$

Using covariant notation the result of Eq. (5) may be expressed in the following form

$$T^{\mu\nu} = \mathcal{E} u^{\mu} u^{\nu} - \mathcal{P} \Delta^{\mu\nu}, \quad (7)$$

where we introduced the symmetric projection operator on the space orthogonal to the fluid four-velocity, $\Delta^{\mu\nu} \equiv g^{\mu\nu} - u^{\mu} u^{\nu}$, which satisfies conditions $u_{\mu} \Delta^{\mu\nu} = 0$, $\Delta_{\alpha}^{\mu} \Delta^{\alpha\nu} = \Delta^{\mu\nu}$ and $\Delta_{\mu}^{\mu} = 3$, and $g^{\mu\nu} = \text{diag}(1, -1, -1, -1)$ is the metric tensor.

Similarly, the Lorentz boost transformation applied to Eq. (4) leads to the following tensor decomposition of N_i^{μ} in the general frame

$$N_i^{\mu} = \mathcal{N}_i u^{\mu}, \quad (8)$$

⁴ Equivalently, instead of the third component of the isospin one may use the electric charge.

so that in the LRF, where $u_{\text{LRF}}^\mu = (1, \mathbf{0}, 0)$, one has $\mathcal{N}_i = N_i^\mu u_{\mu, \text{LRF}}$.

Equation (1) may be rewritten in a somewhat more familiar form using Eq. (7) and performing projections perpendicular and parallel to the fluid four-velocity

$$\Delta_\nu^\alpha \partial_\mu T^{\mu\nu} = (\mathcal{E} + \mathcal{P}) Du^\alpha - \nabla^\alpha \mathcal{P} = 0, \quad (9)$$

$$u_\nu \partial_\mu T^{\mu\nu} = D\mathcal{E} + (\mathcal{E} + \mathcal{P})\theta = 0, \quad (10)$$

where $D \equiv u^\mu \partial_\mu$ is the co-moving time derivative, $\nabla^\mu \equiv \Delta^{\mu\alpha} \partial_\alpha$ is the spacial gradient, and $\theta \equiv \partial_\mu u^\mu$ is the expansion scalar. Equations (9)-(10) are relativistic analogs of the Euler and continuity equations, respectively. Similarly, putting decompositions (8) in Eqs. (2) yields

$$\partial_\mu N_i^\mu = D\mathcal{N}_i + \mathcal{N}_i\theta = 0. \quad (11)$$

Equations (9)-(11) contain together $4 + N$ independent partial differential equations for the space-time evolution of $5 + N$ quantities (three components of four-velocity, energy density, pressure and N charge densities). In order for the system to be closed one has to introduce a material-specific *equation of state* relating the pressure, the energy density and the charge densities in the system, $\mathcal{P} = \mathcal{P}(\mathcal{E}, \mathcal{N}_i)$. Since the system is locally in equilibrium such a relation exists and has to follow from the underlying microscopic theory describing the system. Henceforth, we will assume that the system created in heavy-ion collisions is charge-free, $\mathcal{N}_i(x) \equiv 0$, which is a reasonable assumption for central rapidity region at the ultra-relativistic energies. The energy density and pressure for the charge-free matter in equilibrium may be directly related to the temperature of the system, $\mathcal{E} = \mathcal{E}(T)$, $\mathcal{P} = \mathcal{P}(T)$, see Sec. 3. A number of studies show that the successful description of the experimental data requires the use of ‘‘cross-over’’-type equation of state of strongly interacting matter with the transition from the quark-gluon plasma phase to the hadron gas phase. For the numerical results presented in the remaining part of these lectures we will use the results of the Ref. [28]. The temperature dependence of the square speed of sound $c_s^2(T) = d\mathcal{P}/d\mathcal{E}$ obtained in Ref. [28] is shown in Fig. 1⁵.

Except for quite limited number of special cases of highly-symmetric flow patterns, such as the Bjorken [29] or Gubser [30] flows, Eqs. (9)-(11) have to be solved numerically. In the case of modeling the collisions at relativistic energies, in which case the system is approximately boost-invariant (with respect to Lorentz boosts along the beam (z) direction) in the central rapidity region, the hydrodynamic evolution is preferably performed in *Milne coordinates* $x^\mu = (\tau, \mathbf{x}_T, \zeta)$ instead of Minkowski coordinates $\tilde{x}^\mu = (t, \mathbf{x}_T, z)$ [29]. The relation between the two is given by the following coordinate transformation

$$t = \tau \cosh \zeta, \quad (12)$$

$$z = \tau \sinh \zeta, \quad (13)$$

⁵ Note that in the case of dissipative fluid dynamics due to the existence of transport coefficients the inclusion of the equation of state is usually more involved [14].

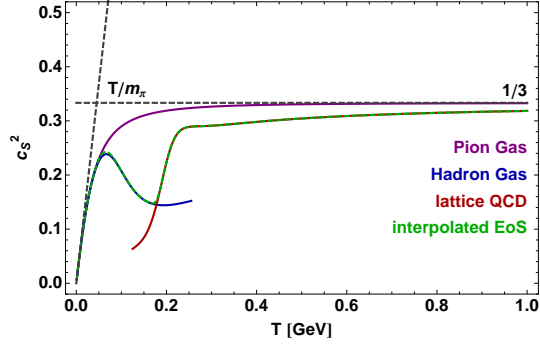


Fig. 1 Temperature dependence of the squared speed of sound $c_s^2 = d\mathcal{P}/d\mathcal{E}$ for the hadron gas, lattice QCD quark-gluon plasma, and interpolation thereof as found in Ref. [28].

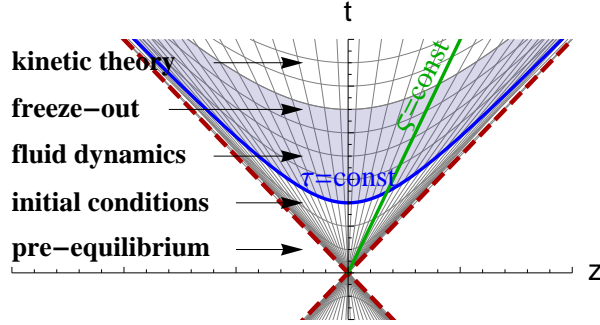


Fig. 2 The Milne coordinates shown in the Minkowski space-time. Directions x and y are suppressed.

with $\tau = \sqrt{t^2 - z^2}$ and $\zeta = \tanh^{-1}(z/t)$ denoting longitudinal proper time and space-time rapidity, respectively; see Fig. 2.

In this coordinate system it is also convenient to parametrize the fluid four-velocity in the following form

$$u^\mu = (u_0 \cosh y_u, \mathbf{u}_T, u_0 \sinh y_u), \quad (14)$$

where y_u is the longitudinal rapidity of the fluid, and $u_0 = \sqrt{1 + u_T^2}$, with $u_T = \sqrt{u_x^2 + u_y^2}$.

3 Fluid dynamics from kinetic theory

It is instructive to see the relation between the fluid dynamics, as a general classical field theory, and the relativistic kinetic theory. The latter is based on the knowledge of the *single-particle distribution function* $f(x, p)$, which is defined through the number of (on-shell) particles dN in the phase-space volume $d^3x d^3p$ located at the phase-space point (x^μ, p^μ) , where $p^\mu = (E_p, \mathbf{p}, p_z)$ with $E_p = \sqrt{m^2 + \mathbf{p}^2 + p_z^2}$. The evolution of $f(x, p)$ follows from the standard relativistic Boltzmann equation

$$p^\alpha \partial_\alpha f = -C[f], \quad (15)$$

where $C[f]$ is the collisional kernel, which, in general, may have highly complicated form. In global equilibrium $f(x, p)$ is stationary, which means that $C[f]$ vanishes in two very different regimes: free-streaming (no interactions) and equilibrium (strongest possible interactions). Often the collisional kernel is treated in the relaxation-time approximation,

$$C[f] = p_\mu u^\mu \frac{f - f_{\text{eq}}}{\tau_{\text{eq}}}, \quad (16)$$

where τ_{eq} is the relaxation time, and f_{eq} is the equilibrium distribution.

Equations of motion for the soft modes of the system, identified with the fluid dynamical sector of the theory, may be derived by taking the lowest- n momentum moments [31, 5, 6],

$$\hat{\mathcal{J}}^{\mu_1 \dots \mu_n} \equiv \int dP p^{\mu_1} p^{\mu_2} \dots p^{\mu_n}, \quad \int dP \equiv \int \frac{d^3p}{E_p}, \quad (17)$$

of the Boltzmann equation (15), which gives

$$\partial_\alpha \mathcal{J}^{\alpha \mu_1 \dots \mu_n} = -\mathcal{C}^{\mu_1 \dots \mu_n}[f], \quad (18)$$

where we defined

$$\mathcal{J}^{\alpha \mu_1 \dots \mu_n} \equiv \hat{\mathcal{J}}^{\alpha \mu_1 \dots \mu_n} f, \quad (19)$$

$$\mathcal{C}^{\mu_1 \dots \mu_n}[f] \equiv \hat{\mathcal{J}}^{\mu_1 \dots \mu_n} C[f]. \quad (20)$$

Explicitly, the first two moments lead to the following set of dynamical equations,

$$\partial_\mu \mathcal{J}^\mu = u_\mu \frac{\mathcal{J}_{\text{eq}}^\mu - \mathcal{J}^\mu}{\tau_{\text{eq}}}, \quad (21)$$

$$\partial_\mu \mathcal{J}^{\mu\nu} = u_\mu \frac{\mathcal{J}_{\text{eq}}^{\mu\nu} - \mathcal{J}^{\mu\nu}}{\tau_{\text{eq}}}. \quad (22)$$

One may immediately identify zeroth and first moments of the distribution function as particle four-current and the energy-momentum tensor,

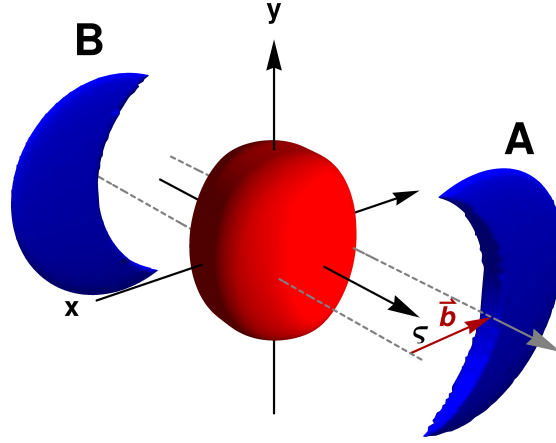


Fig. 3 The geometry of heavy-ion collision in the Milne coordinates.

$$N^\mu \equiv \mathcal{J}^\mu \quad (23)$$

$$T^{\mu\nu} \equiv \mathcal{J}^{\mu\nu}. \quad (24)$$

The conservation of particle current $u_\mu(\mathcal{J}_{\text{eq}}^\mu - \mathcal{J}^\mu) = 0$, and energy-momentum tensor $u_\mu(\mathcal{J}_{\text{eq}}^{\mu\nu} - \mathcal{J}^{\mu\nu}) = 0$ thus leads to Eqs. (1)-(2).

Using decompositions of the particle four-current (8) and the energy-momentum tensor (7), and the knowledge of the LTE distribution function $f_{\text{eq}} = f(p_\mu u^\mu, T, \mu_i)$, see Eq. (45) in Sec. 8, one may find explicit forms of the thermodynamic variables, $\mathcal{E} = \mathcal{E}(T, \mu_i)$, $\mathcal{P} = \mathcal{P}(T, \mu_i)$, and $\mathcal{N} = \mathcal{N}(T, \mu_i)$. The latter define the equation of state of the system within kinetic theory. For the conformal charge-free system one gets $\mathcal{E}(T) = 3\mathcal{P}(T) = 3T\mathcal{N}(T) \sim T^4$ [24].

4 Event-averaged initial conditions for fluid dynamics

In general, Eqs. (9)-(11) have to be supplemented with proper *initial conditions*, specified on the hypersurface of constant longitudinal proper time $\tau = \tau_i$, which usually defines beginning of the fluid dynamical evolution. In particular, one has to provide $\mathcal{E}(\tau_i, \mathbf{x}_T, \zeta)$, $u_x(\tau_i, \mathbf{x}_T, \zeta)$, $u_y(\tau_i, \mathbf{x}_T, \zeta)$, $y_u(\tau_i, \mathbf{x}_T, \zeta)$, and $\mathcal{N}_i(\tau_i, \mathbf{x}_T, \zeta)$. These should follow from some microscopic models of the initial state created in heavy-ion collision, though usually they are, to some extent, just fitted to reproduce the data.

For the initial energy density profile, we will use the *tilted source* model [32] of the initial state, which was applied quite successfully to describe various experimental observables measured at RHIC, including the so called directed flow v_1

component of the Fourier decomposition of the azimuthal particle spectra. The initial energy density profile within this model is proportional to the density of sources $n(\mathbf{x}_T, \zeta, b)$

$$\mathcal{E}(\tau_i, \mathbf{x}_T, \zeta, b) = \mathcal{E}_i \frac{n(\mathbf{x}_T, \zeta, b)}{n(\mathbf{0}, \mathbf{0}, 0)}, \quad (25)$$

where

$$n(\mathbf{x}_T, \zeta, b) = G(\zeta) \left\{ (1 - \kappa) \left[W_A(\mathbf{x}_T, b) F(\zeta) + W_B(\mathbf{x}_T, b) F(-\zeta) \right] + \kappa B(\mathbf{x}_T, b) \right\}. \quad (26)$$

The functions $W_{A(B)}$, and B are the density of wounded nucleons from the nucleus A (B), and the density of binary collisions, respectively, both specified at a certain value of the impact parameter $b = |\mathbf{b}|$, see Fig. 3. These quantities are determined entirely from the optical limit of the *Glauber model* [33]. The admixture of binary collisions is controlled by the parameter $\kappa = 0.14$ that is typically fitted to reproduce the centrality dependence of charge hadron multiplicity. As herein we assume that the system is charge-free, $\mathcal{N}_i(\tau_i, x, y, \zeta) \equiv 0$, the initial central energy density \mathcal{E}_i of the system may be translated to its initial central temperature $T_i = T_i(\mathcal{E}_i)$, which is fitted to reproduce the total number of charged particles produced in the experiment.

The functional form of the density profile in rapidity in Eq. (26) is

$$G(\zeta) \equiv \exp \left[-\frac{(\zeta - \Delta\zeta)^2}{2\sigma_\zeta^2} \Theta(|\zeta| - \Delta\zeta) \right]. \quad (27)$$

The parameters in Eq. (27) are deduced from the fits to the final rapidity spectrum of charged hadrons. For RHIC the fit results in $\Delta\zeta = 2.3$ and $\sigma_\zeta = 1.6$. The tilt of the source results from the preferred particle emission from the moving participant nucleon into its forward hemisphere, and may be parametrized as follows [32]

$$F(\zeta) = \begin{cases} 0 & \zeta < -y_N, \\ (\zeta + y_N)/(2y_N) & \text{if } -y_N \leq \zeta \leq y_N, \\ 1 & \zeta > y_N, \end{cases} \quad (28)$$

where $y_N = \log(2\sqrt{s_{NN}}/m_N) - \zeta_{\text{shift}}$ is the nucleon rapidity shifted by the value $\zeta_{\text{shift}} = 2$ (treated as a phenomenological parameter), $\sqrt{s_{NN}}$ is the center-of-mass energy per nucleon pair, and m_N is the nucleon mass. The resulting initial temperature profile in $x - y$ plane and $x - \zeta$ plane is shown in bottom panels of Fig. 4, respectively.

Finally, the flow in the transverse plane, as usual, is assumed to vanish initially, $u_x(\tau_i, \mathbf{x}_T, \zeta) = 0$, $u_y(\tau_i, \mathbf{x}_T, \zeta) = 0$, and the flow in the longitudinal direction is assumed to have the Bjorken-type scaling form $y_u(\tau_i, \mathbf{x}_T, \zeta) = \zeta$.

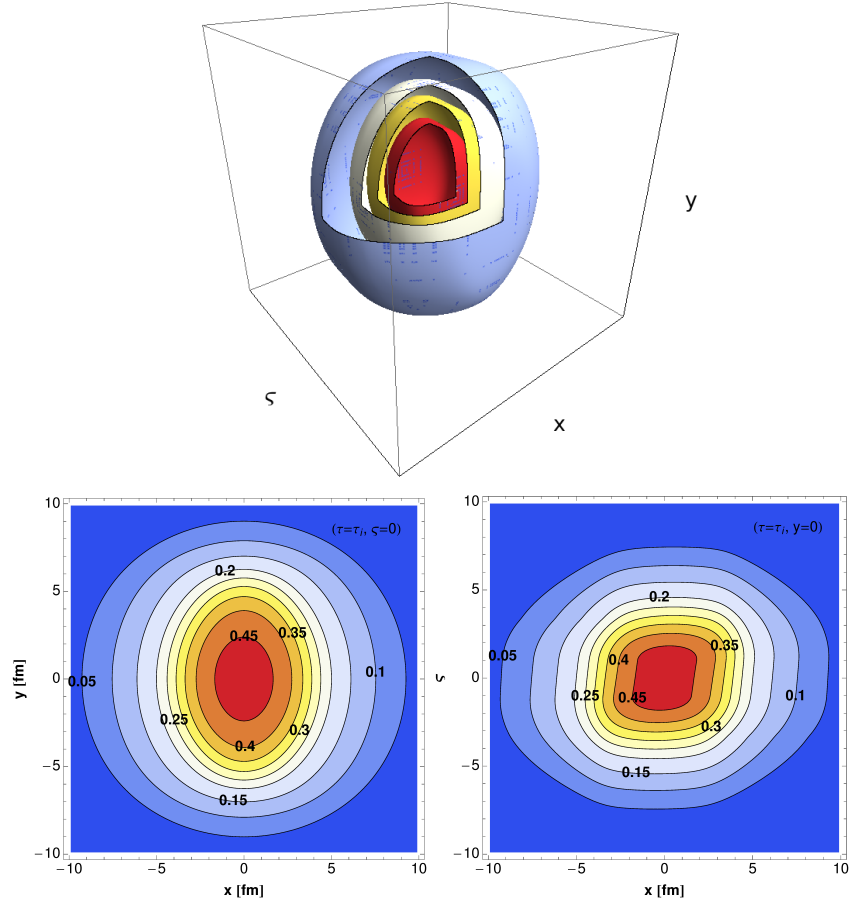


Fig. 4 (Top panel) The isothermal surfaces ($T \in \{0.4, 0.3, 0.2, 0.1\}$ GeV) of the tilted source in the Milne coordinates. (Bottom panels) The isothermal contours of the initial temperature profile of fluid dynamic evolution in the Milne coordinates in x - y (left) and x - ζ (right) plane.

5 Particle decoupling

Relativistic perfect fluid dynamics describes, by definition, the infinitely strongly-coupled system of particles evolving from one local thermal equilibrium state to another. When applied to relativistic heavy-ion collisions one immediately realizes that the latter assumption breaks down as the evolution proceeds. The rapid expansion of the created fireball into the vacuum leads to its cooling and dilu-

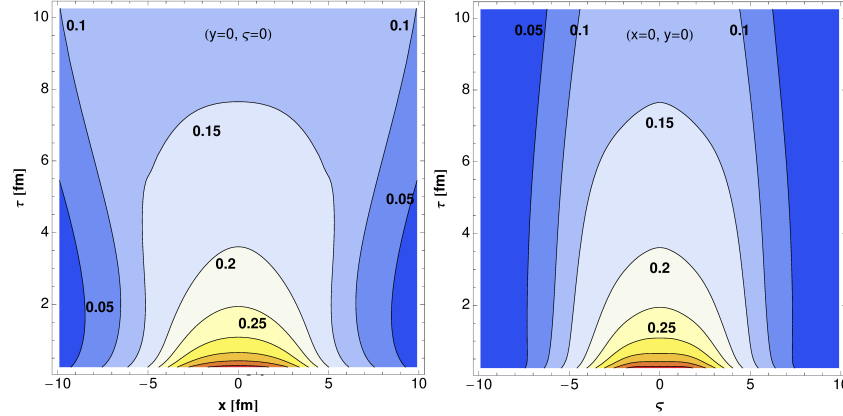


Fig. 5 The isothermal contours of the fluid dynamical evolution in the Milne coordinates.

tion, see Fig. 5. Eventually, the particle scatterings become too rare to prevent the particles from leaving the fluid. As a result the local thermal equilibrium cannot be maintained anymore and the fluid description breaks down. This complicated gradual process of particle decoupling from the fluid is often called the *freeze-out* [20, 21, 22, 23, 24, 25, 26, 27].

As the interactions cease and the system becomes rarefied the kinetic theory description in terms of hadronic degrees of freedom and scattering cross sections becomes more adequate. A possible way to describe this process is to compare locally the time scale of the expansion of the fluid τ_{exp} (which drives the system out of equilibrium), and the time scale characterizing collisions between the particles τ_{coll}^k (which tend to restore it) [34]. In the differential form, the decoupling may be formulated as the following inequality [35]

$$\tau_{\text{coll}}^k \geq \tau_{\text{exp}}, \quad (29)$$

where $\tau_{\text{exp}} \sim 1/\theta(x)$ (see Sec. 2), and $\tau_{\text{coll}}^k \sim 1/\sum_l \langle \sigma_{kl} v_{kl} \rangle \tilde{\mathcal{N}}_l^k(x)$, with σ_{kl} denoting the scattering cross section between the particle species k and l , v_{kl} being their relative velocity in the center of mass frame, and $\tilde{\mathcal{N}}_l^k(x)$ describing respective particle densities. If the condition (29) is satisfied the particle species k start to decouple from the fluid.

A few comments are in order here:

- Both, the flow velocity $u^\mu(x)$ and particle densities $\tilde{\mathcal{N}}_l^k(x)$ are, in general, space-time dependent quantities, which means that the freeze-out process begins at different space-time points of the fluid.
- In general, the cross sections σ_{kl} depend on the particle species, thus some particle species decouple “before” others. In the case of ultra-relativistic heavy-ion collisions the scattering cross section is usually dominated by a single species (pions), whose freeze-out triggers others.

- In perfect fluid dynamics, to which we restrict ourselves, the particle density $\mathcal{N}_i(x) \sim T^3(x)$. As a result, the condition (29) is usually significantly simplified to the condition of temperature dropping below a certain freeze-out temperature [21]

$$T_{\text{freeze}} \geq T(x). \quad (30)$$

- The total cross section $\sigma_{kl} = \sigma_{kl}^{\text{el}} + \sigma_{kl}^{\text{in}}$ is always larger than the elastic one σ_{kl}^{el} , which implies that the particle-number changing processes cease before the momentum changing processes. This results in the distinction between the *chemical freeze-out* (inelastic collisions stop), and the *kinetic/thermal freeze-out* (elastic collisions stop). It means that, typically, chemical freeze-out takes place at higher temperature than the thermal one,

$$T_{\text{chem}} \geq T_{\text{therm}}. \quad (31)$$

- Equation (29) may, in general, involve additional unknown parameter of the order of 1, which sets the overall scale for the freeze-out processes [35].

6 Single-freeze-out scenario

The dynamical description of the particle decoupling according to Eq. (29) is quite difficult to realize in practice. Instead, usually a significant simplification of the freeze-out dynamics, often called the *single-freeze-out* model, is adopted [36, 37, 38, 39, 40, 41, 42]. The latter relies on the assumption that the chemical and thermal freeze-out occur simultaneously. Within this framework one assumes that once the temperature $T(x)$ in the fluid decreases locally below a certain value T_{freeze} all particle species decouple completely from the fluid⁶. Mathematically, the condition $T(x) = T_{\text{freeze}}$ defines a three-dimensional freeze-out hypersurface Σ in the four-dimensional Minkowski space-time \mathcal{M} (see Sec. 7). The thickness of Σ is idealistically assumed to be infinitesimal, which means that the freeze-out process takes place instantaneously. Just before crossing Σ , in the fluid phase, the matter is considered to be in local thermal and chemical equilibrium, so that phase-space distributions of the microscopic constituents follow the statistical ones (see Sec. 8). It is assumed that freeze-out process itself, due to its instantaneous character, does not affect the phase-space distributions, so that equilibrium distributions are also shared by the particles emitted from the surface Σ .

Outside the fluid region various approximations, usually based on some sort of transport theory, may apply. In the original single-freeze-out model [36, 37, 38] the particles created on Σ , termed as *primordial*, are assumed to form *ideal non-interacting gas of hadrons*, which undergo *free-streaming* to the detectors. However,

⁶ Although the assumption of isothermal freeze-out seems to be crude, it was shown to give a quite reasonable approximation of the differential freeze-out condition, Eq. (29) [21, 22].

the (primordial) hadron gas contains the full mass spectrum of hadronic resonances, which subsequently decay into *stable* particles⁷. Due to decays, the abundances of stable particles, as well as their spectra, are modified (see Sec. 10). As a result, the temperature T_{freeze} should, in general, be interpreted as a *switching temperature* (from fluid to particle description), rather than the true chemical and kinetic freeze-out temperature. Another possibility is to perform the switching at somewhat higher, often called *particlization* [43], temperature $T_{\text{part}} > T_{\text{freeze}}$, when the system is considered to be still strongly interacting, but the transport theory description is more adequate. The particle ensemble, together with their phase-space coordinates, is then passed to the quantum molecular transport models describing various phenomena in the dense hadronic medium. For the sake of simplicity, in this work we focus on the *single-freeze-out* scenario solely.

Finally, one should note here that it is commonly assumed that the fluid dynamical description applies to the whole forward light-cone of the system and a *posteriori* part of the space-time evolution of fluid satisfying $T(x) < T_{\text{freeze}}$ is neglected and replaced with the transport theory description. This procedure obviously introduces some inconsistency at the boundary Σ , as outside the fluid regime the system is a non-interacting hadron gas (as opposed to the strongly-interacting fluid). Consequently, the boundary conditions at Σ for the fluid evolution are different in the two cases. Possible consequences of these problems will be neglected herein. We will only note here, that these problems may be largely reduced when large anisotropies are included already within fluid dynamics stage which would describe its gradual break up [2, 3, 4]. In this way the switching should introduce less uncertainty.

7 Freeze-out hypersurface extraction

When initialized with proper initial conditions the perfect fluid dynamics determines the evolution of the temperature, flow velocity, and the chemical potentials (if charge conserving theory is considered) in the entire forward light-cone of the Minkowski space-time \mathcal{M} , whose points satisfy the requirement $\tau \geq \tau_i$. Usually, due to specific shape of the isothermal freeze-out hypersurface Σ (see Figs. 5 and 6), it is convenient to parametrize the ambient space-time \mathcal{M} with three angles, say θ , ζ and ϕ , and the distance ρ from the coordinate system's origin ($\tau = \tau_i, x = 0, y = 0, \zeta = 0$)⁸. The resulting parametrization reads [44, 45]

$$x^0 = t(\rho, \theta, \zeta, \phi) = \tau \cosh \zeta, \quad (32)$$

$$x^1 = x(\rho, \theta, \zeta, \phi) = r \sin \theta \cos \phi, \quad (33)$$

$$x^2 = y(\rho, \theta, \zeta, \phi) = r \sin \theta \sin \phi, \quad (34)$$

$$x^3 = z(\rho, \theta, \zeta, \phi) = \tau \sinh \zeta, \quad (35)$$

⁷ The inverse processes, due to low probabilities, are usually neglected in this framework.

⁸ Note from Figs. 5 and 6 that τ is not always a function of remaining space-time coordinates.

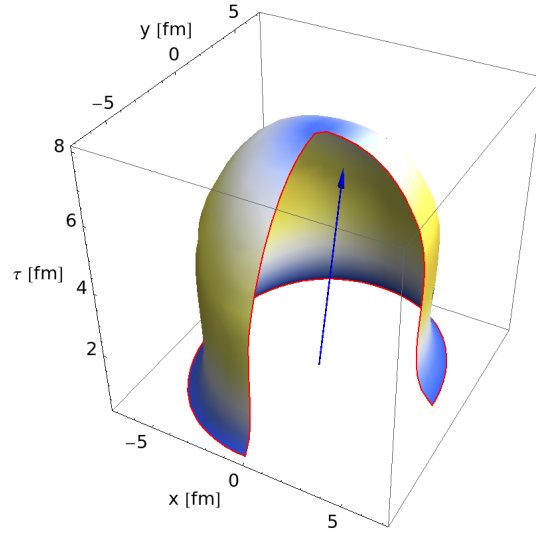


Fig. 6 Isothermal freeze-out surface in Milne coordinates ($\zeta = 0$).

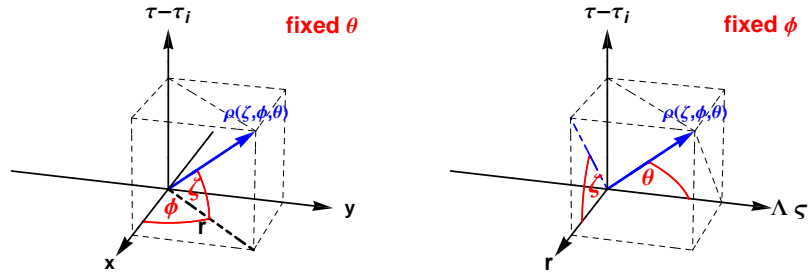


Fig. 7 Space-time parametrization with angles θ , ζ and ϕ , and the distance ρ .

with

$$\Lambda \zeta = \rho \cos \theta, \quad (36)$$

$$r = \rho \cos \zeta, \quad (37)$$

so that $\tau - \tau_i = \rho \sin \theta \sin \zeta$, and

$$0 \leq \zeta \leq \pi/2, \quad 0 \leq \phi < 2\pi, \quad \text{and} \quad 0 \leq \theta \leq \pi; \quad (38)$$

see Fig. 7. The isothermal freeze-out condition defines the hypersurface Σ embedded in \mathcal{M} in the following way

$$\Sigma(\theta, \zeta, \phi) = \{x \in \mathcal{M} : T(\rho, \theta, \zeta, \phi) = T_{\text{freeze}}\}, \quad (39)$$

so that one has implicitly $\rho = \rho(\theta, \zeta, \phi)$. One should note here that, while at Σ , by definition, the temperature is fixed, the flow four-velocity is not, $u^\mu = u^\mu(\theta, \zeta, \phi)$. The infinitesimal element of the hypersurface Σ is defined by the covariant four-vector [17]

$$d^3\Sigma_\mu = \varepsilon_{\mu\alpha\beta\gamma} \frac{\partial x^\alpha}{\partial \zeta} \frac{\partial x^\beta}{\partial \phi} \frac{\partial x^\gamma}{\partial \theta} d\zeta d\phi d\theta, \quad (40)$$

where $\varepsilon_{\mu\alpha\beta\gamma}$ is the totally antisymmetric tensor in four dimensions with $\varepsilon_{0123} = +1$.

8 Cooper-Frye formalism

The change from fluid elements to hadrons at the switching hypersurface $\Sigma(x)$ is usually performed with the use of kinetic theory concepts. In the transport theory framework the flux of particle species k is expressed with the formula (see Eqs. (19) and (23)) [21]

$$N_k^\mu(x) = \int \frac{d^3p}{E_p} p^\mu f_k(x, p), \quad (41)$$

where $p^\mu = (E_p, \mathbf{p}, p_z)$ is the four-momentum of the (on-shell) particle with mass m_k , and $f_k(x, p)$ is its phase-space distribution function. The number of world-lines of particles of species k crossing the infinitesimal element $d^3\Sigma$ of the surface Σ is then calculated from the expression

$$N_\Sigma^k \equiv d^3\Sigma_\mu N_k^\mu = \int \frac{d^3p}{E_p} d^3\Sigma_\mu p^\mu f_k(x, p). \quad (42)$$

The invariant momentum spectrum of particles produced at the surface element $d^3\Sigma$ is

$$E_p \frac{dN_\Sigma^k}{d^3p} = d^3\Sigma_\mu p^\mu f_k(x, p). \quad (43)$$

Therefore, the invariant momentum distribution of hadrons emitted on the entire freeze-out hypersurface Σ is given by the integral

$$E_p \frac{dN^k}{d^3p} = \int_\Sigma d^3\Sigma_\mu p^\mu f_k(x, p). \quad (44)$$

Equation (44) is commonly known as the Cooper-Frye formula [46].

It is usually assumed that just before decoupling from the fluid, *i.e.*, before the particles cross the switching surface Σ , they are in local thermal and chemical equilibrium such that their phase-space distributions are described by the equilibrium ones. In such a case one assumes that produced hadrons follow either Fermi–Dirac ($a = -1$) or Bose–Einstein ($a = +1$) distributions,

$$f_k(x, p) = f_k(p_\mu u^\mu(x), T(x), \tilde{\mu}_k) = \frac{g_k}{(2\pi)^3} \left\{ \exp \left[\frac{p_\mu u^\mu(x) - \tilde{\mu}_k(x)}{T(x)} \right] - a \right\}^{-1}, \quad (45)$$

where the factor $g_k = 2s_k + 1$ takes into account the spin degeneracy of hadron species k . The chemical potential $\tilde{\mu}_k$ is given by the linear combination of the chemical potentials μ_i (see Sec. 2) and the respective charges of the hadron species k

$$\tilde{\mu}_k = \sum_i Q_i^k \mu_i. \quad (46)$$

The particle's four-momentum, as measured by the experiment, is usually parametrized in the following way

$$p^\mu = (m_T \cosh y_p, p_T \cos \phi_p, p_T \sin \phi_p, m_T \sinh y_p), \quad (47)$$

where $p_T = \sqrt{p_x^2 + p_y^2}$ is the transverse momentum, $m_T = \sqrt{p_T^2 + m_k^2}$ is the transverse mass, $y_p = \ln[(E_p + p_z)/(E_p - p_z)]/2$ is the longitudinal rapidity and $\phi_p = \tan^{-1}(p_y/p_x)$ is the momentum azimuthal angle in the plane transverse to the beam axis.

With definitions introduced above the integration measure $d^3\Sigma_\mu p^\mu$ in Eq. (44) takes the form

$$\begin{aligned} d^3\Sigma_\mu p^\mu &= \frac{\sin \theta \tau \rho^2}{\Lambda} \left[\frac{\partial \rho}{\partial \zeta} \cos \zeta (p_T \sin \zeta \cos(\phi_p - \phi) - m_T \cos \zeta \cosh(y_p - \zeta)) \right. \\ &\quad + \cos \zeta \sin \theta \left(\rho \sin \theta - \frac{\partial \rho}{\partial \theta} \cos \theta \right) \\ &\quad \times (p_T \cos \zeta \cos(\phi_p - \phi) + m_T \sin \zeta \cosh(y_p - \zeta)) \\ &\quad + \cos \zeta \sin \theta \left(\rho \cos \theta + \frac{\partial \rho}{\partial \theta} \sin \theta \right) \frac{\Lambda}{\tau} m_T \sinh(y_p - \zeta) \\ &\quad \left. - \frac{\partial \rho}{\partial \phi} p_T \sin(\phi_p - \phi) \right] d\zeta d\phi d\theta \equiv h_k(\zeta, \phi, \theta, p_T, \phi_p, y_p) d\zeta d\phi d\theta, \quad (48) \end{aligned}$$

and the (Lorentz-boosted) energy is

$$p_\mu u^\mu = u_0 m_T \cosh(y_p - y_u) - p_T u_T \cos(\phi_p - \phi_u), \quad (49)$$

where we introduced yet another variable ϕ_u such that $u_x = u_T \cos \phi_u$ and $u_y = u_T \sin \phi_u$. One should note that in cases where some symmetries are present in the system the formulas (48)-(49) may be respectively simplified [24, 47]. Using expressions (48)-(49) in the Cooper-Frye formula (44) one obtains a six-dimensional particle distribution, which can be used directly to generate particles (both, stable hadrons and unstable resonances) on Σ

$$\frac{d^6 N^k}{p_T d p_T d \phi_p d y_p d \zeta d \phi d \theta} = \frac{g_k}{(2\pi)^3} h_k(\zeta, \phi, \theta, p_T, \phi_p, y_p) f_k(\zeta, \phi, \theta, p_T, \phi_p, y_p)$$

$$\equiv \mathcal{F}_k(\zeta, \phi, \theta, p_T, \phi_p, y_p). \quad (50)$$

The Cooper-Frye formula, Eq. (44), is nowadays commonly used in the fluid dynamical simulations of the heavy-ion collisions to describe hadron production on the freeze-out hypersurface. There are, however, well known limitations of this prescription. An immediate problem with Eq. (44) arises if the freeze-out hypersurface contains both time-like and space-like parts. In particular, if the freeze-out element is time-like, so that associated normal vector is space-like, for certain directions of the momentum p^μ the invariant measure $d^3\Sigma_\mu p^\mu$ may be negative. Thus, the particle number generated in this region will become ill-defined (the Cooper-Frye formula would in such a case describe the back-flow of particles into the fluid) [21]. One may show that at high energies the negative emission is usually negligible [48], so that it may be safely removed by introducing the step function $\Theta(d^3\Sigma_\mu p^\mu)$ on the right-hand side of Eq. (44) [21]. Another issue connected with Eq. (44) is its insensitivity to the fact that particles with large momenta are in general more probable to leave the fluid more easily than the soft ones [22].

9 Hadron abundances

For the system in local thermal equilibrium the flux N_k^μ of particle species k from the fluid cell is proportional to its four-velocity, see Eq. (8). In this case, using formula (42), the total number of particles emitted on the entire hypersurface may be expressed as follows

$$N_k \equiv \int_\Sigma d^3\Sigma_\mu N_k^\mu = \int_\Sigma d^3\Sigma_\mu u^\mu(x) \mathcal{N}_k(T(x), \tilde{\mu}_k(x)). \quad (51)$$

One should stress here that the particle density \mathcal{N}_k in Eq. (51) is expressed solely through the local temperature $T(x)$ and chemical potentials $\tilde{\mu}_k(x)$. It is straightforward to see that, if T and $\tilde{\mu}_k$ are constant along Σ , the integral of the flow pattern on the freeze-out manifold factorizes in Eq. (51), giving the so called effective comoving volume $V_{\text{eff}} \equiv \int_\Sigma d^3\Sigma_\mu u^\mu(x)$. When one considers ratios of particle multiplicities of different species, say a and b , the factor V_{eff} cancels out completely in the ratios [49, 50] giving

$$\frac{N_a}{N_b} = \frac{\mathcal{N}_a(T, \tilde{\mu}_k)}{\mathcal{N}_b(T, \tilde{\mu}_k)}. \quad (52)$$

Arguments presented above gave rise to the wide variety of analyses under the common name of *thermal* or *statistical* models [51, 52, 53, 54, 55]. They focus mainly on the extraction of thermodynamic properties of the matter at the chemical freeze-out based on thermal analysis of the multiplicities of the experimentally measured particles and ratios thereof. Using the grand canonical version of the thermal approach the fits usually yield the chemical freeze-out temperature of the order of the quark-hadron phase transition obtained from the lattice QCD calculations

$$T_{\text{chem}} \sim T_c \sim 170 \text{ MeV}, \quad (53)$$

which suggest possible relation between hadronization process and chemical equilibration [56]⁹.

Equation (52) requires a few important remarks: (i) the integrals quoted above are performed over the full momentum space, which means that the reliable analysis would require the 4π acceptance for identified particles, (ii) at low energies and forward rapidities the freeze-out conditions are usually quite different from the baryon-free midrapidity region, suggesting that thermal analyses based on Eq. (52) yield, in this case, only approximate (averaged over the entire hypersurface) values of thermal parameters at freeze-out. Nevertheless, keeping in mind its simplicity, the precision of the thermal approach is quite remarkable.

10 Decays of resonances

When discussing the thermal/statistical approach we neglected an important aspect of the modeling connected with the role of resonances. It is usually assumed that the particles created at freeze-out form an ideal non-interacting gas of hadrons, which includes, in principle, entire mass spectrum of unstable resonances. In reality, the latter subsequently decay populating the spectrum of stable hadrons, which is then observed in the detector. Although the Boltzmann factor tends to suppress heavy states, one should keep in mind that, according to the Hagedorn hypothesis [58], their mass spectrum increases exponentially. While at low temperatures the role of the resonance feed-down is diminished, at the temperatures of the order of T_{chem} it is quite significant. In fact, the successful description of the available data on the hadronic abundances within the statistical approach, as quoted in Sec. 9, was possible largely due to inclusion of the full mass spectrum of the hadronic resonances [59]¹⁰.

As it was shown within the so called Cracow model [37] (see next Section), which includes hydrodynamic-like expansion of the system, the role of the resonance feed-down turns out to be equally important for description of the momentum spectra of stable hadrons as the flow itself. This is mainly due to the fact that decays of heavy resonances populate mainly the soft region of the stable hadron transverse-momentum spectra leading to their steeper slopes. Effectively, the observed inverse slope parameter, usually interpreted as the thermal freeze-out temperature, is much smaller than the chemical freeze-out temperature inferred from the analysis of the hadronic ratios

$$T_{\text{therm}} \sim 130 \text{ MeV}; \quad (54)$$

⁹ Note that the new lattice QCD simulations suggest somewhat lower values the critical temperature, $T_c \sim 155 \text{ MeV}$ [57].

¹⁰ In practice, all resonances from the Particle Data Group tables [59], whose properties are known well enough, were included.

compare Eq. (53). This observation gave further support to the single-freeze-out model, and explained apparent mismatch between the two freeze-out temperatures.

11 Hydro-inspired parameterizations of freeze-out

According to Eq. (45) the spectrum of particles produced in a single fluid cell is thermal. However, even if the thermal parameters T and $\tilde{\mu}$ are constant along the Σ , the total momentum spectrum, as calculated with Eq. (44), includes contributions from different fluid cells, each boosted with a different velocity $u^\mu(x)$. Therefore, the resulting total spectrum is modified due to the combination of *redshift* and *blueshift* effects [36]. These effects are observed in the experiment in the form of the characteristic concave shape of the transverse momentum spectrum. In view of these arguments, the realistic description of the momentum spectra of stable hadrons must include effects of some kind of collective evolution reflected in the finite flow of the matter at freeze-out.

The most natural way to include flow at the freeze-out is to perform full fluid dynamical simulations along the lines presented in Sec. 2. Unfortunately, numerical solution of fluid dynamical equations of motion is rather complicated and computationally intensive. Moreover, fluid evolution requires at least *some* knowledge of the initial conditions, which are rather poorly known, and thus always bias final results. In order to avoid such problems, one may follow a different strategy, which results in the so called *hydro-inspired* models. Within these models the conditions at the freeze-out hypersurface ($T(x), u^\mu(x), \mu_i(x)$), as well as the shape of the freeze-out surface $\Sigma(x)$, are simply assumed, or *inspired*, by the full numerical fluid dynamical simulations. Among these models the most successful ones are the Blast-wave [42, 60] and Cracow [36] models.

In particular, within the Cracow model [36] (as well as in Blast-wave model) it is assumed that the freeze-out takes place at the boost-invariant and cylindrically symmetric (in the transverse $x-y$ plane). The hypersurface Σ is defined by the requirement that the particles freeze-out at the surface of constant proper-time ($\tilde{\tau}$)

$$\tilde{\tau}^2 = x^\mu x_\mu = t^2 - x^2 - y^2 - z^2 = \tau^2 - r^2 = \tilde{\tau}_{\text{freeze}}^2 = \text{const.} \quad (55)$$

According to Eq. (55) the particles decouple starting from the center of the *fire-cylinder* towards its edge, so that $0 \leq r \leq r_{\text{max}}$. At the same time the fluid four-velocity is assumed to have the Hubble-like form [61]

$$u^\mu = \gamma(1, \mathbf{v}_T, v_z) = \frac{x^\mu}{\tilde{\tau}_{\text{freeze}}}, \quad (56)$$

which leads to

$$p_\mu u^\mu = \frac{\sqrt{\tilde{\tau}_{\text{freeze}}^2 + r^2}}{\tilde{\tau}_{\text{freeze}}} m_T \cosh(y_p - \zeta) - p_T \frac{r}{\tilde{\tau}_{\text{freeze}}} \cos(\phi_p - \phi), \quad (57)$$

compare Eq. (49). Conditions (55) and (56) imply that the freeze-out hypersurface element is proportional to four-velocity

$$d^3\Sigma = u^\mu \tilde{\tau}_{\text{freeze}} r dr d\zeta d\phi. \quad (58)$$

Within the Cracow model, and with the inclusion of all known hadronic resonances, it was possible to describe, both, the particle ratios and spectra of particles [37], within the single framework.

Due to the fast increase of the computer power during the last decade the full numerical solutions of fluid dynamical evolution equations, including the dissipative effects became easily achievable. As a result the importance of hydro-inspired models was largely reduced, making them useful tools for the estimate of flow and thermal properties at the freeze-out mainly in the analyses of the experimental data; although see [62].

12 Monte-Carlo statistical hadronization

Careful analysis of the experimental data on flow and correlations measured at RHIC and the LHC energies has shown that the realistic description of the dynamics of heavy-ion collisions requires, an experimental-wise, *event-by-event* simulations of such reactions. Due to event-by-event initial state fluctuations (of different kind), such a modeling usually involves running fluid dynamical evolution separately for each event. As a result, in each event the flow patterns at Σ , as well as the shape of the Σ , does not exhibit any symmetries. Hence, in general, the calculation of the particle spectra using Cooper-Frye formula, Eq. (44), has to be done entirely numerically. Moreover, precision studies usually require various experimental cuts and feed-down corrections to be applied to reproduce the data correctly. Thus, it is crucial to have the access to the full information on phase-space properties of the produced hadrons ¹¹. In view of these arguments, the development of Monte-Carlo generators for simulation of physical events became necessary. One of the first numerical open-source codes devoted to this task was THERMINATOR (THERMal heavy-IoN generATOR) [63] (for its new, extended version – THERMINATOR2 – see [48] ¹²).

The THERMINATOR's main functionality is to perform hadronization in relativistic heavy-ion collisions using concepts of the statistical approach and the single-freeze-out model. In its latest version [48], the code performs event-by-event generation of an ensemble of particles (an equivalent of the physical event) given any

¹¹ The access to the entire phase-space properties of the created particle ensemble is of great importance (note that the experimental analysis may access only the four-momentum properties of the particles). As a result, one may, for instance, relate the experimental-wise calculated HBT radii of the system with its *actual* space-time size in simulations.

¹² The THERMINATOR2 code [48] was also supplemented with another (separate) code, FEMTO-THERMINATOR, which is provided to carry out the analysis of the pion-pion femtoscopic correlations.

freeze-out conditions (shape of the hypersurface, flow, and thermodynamic parameters) typically created in fluid dynamic models using the Cooper-Frye formula (44). Within the code one may choose, either one of the predefined hydro-inspired freeze-out parameterizations (such as Blast-wave, or Cracow; see Sec. 11) or an output from any realistic fluid dynamical simulations. Since nowadays the fluid dynamical modeling became the common standard in the field of heavy-ion collisions (at least with event-averaged initial conditions), in what follows we focus mainly on the latter case.

In the case of using directly the fluid dynamics simulations, at first the freeze-out has to be extracted from the fluid evolution, which is out of the scope of THERMINATOR code. In particular, in the case of perfect fluid dynamics, one has to supply the distance $\rho(\zeta, \phi, \theta)$, the components of the flow velocity $u_x(\zeta, \phi, \theta)$, $u_y(\zeta, \phi, \theta)$ and $y_u(\zeta, \phi, \theta)$, temperature $T(\zeta, \phi, \theta)$, and chemical potentials $\mu_i(\zeta, \phi, \theta)$ (although the values of chemical potentials are usually neglected in the hydrodynamic stage)¹³. For the perfect fluid case, it is assumed that on the hypersurface $\Sigma(x)$ the system is in local thermal and chemical equilibrium, which means that the phase-space distributions of the particles have the forms given by Eq. (45)¹⁴.

The THERMINATOR's code is written in an object-oriented C++ programming language and conforms to the CERN's ROOT framework standards [64]. Once the proper input is provided, the generation of hadrons (stable ones and resonances) is done using straightforward Monte Carlo method according to the Cooper-Frye formula (50). The detailed description of the THERMINATOR's theoretical background, code structure, functionalities, as well as short introduction to its usage may be found in the original papers [63, 48], and on the project's website [65]. Herein we will just briefly review its main aspects.

Each evaluation of the code is performed in two stages. The first (preliminary) stage, which is performed once per set of parameters, for each particle species, and whose results are recorded and used for all subsequently generated events, involves:

- Calculation of the global maximum \mathcal{F}_{\max}^k of the right-hand side of Eq. (50).
- Calculation of the average multiplicity \bar{N}_k by integrating Eq. (50) over the entire phase-space (*i.e.* over $\zeta, \phi, \theta, p_T, \phi_p$ and y_p).

The second (main) stage consists of generation of (primordial) particle ensemble and performing decays of unstable resonances, which proceeds on event-by-event basis. In each event:

- It is assumed that the generated ensemble of particles corresponds to the grand canonical ensemble. Hence, the number N_k of particles of species k in the event is generated randomly according to the probability expressed by the Poisson distribution

¹³ In the case of isothermal freeze-out the temperature $T(\zeta, \phi, \theta) = T_{\text{freeze}}$ is constant. Chemical potentials are usually included at the freeze-out, based on the results from the thermal model fits $\mu_i(\zeta, \phi, \theta)$.

¹⁴ In the case of using output from the dissipative fluid dynamics one should correct the distribution function (45) for the non-equilibrium effects as well as supply the THERMINATOR2 code with the respective dissipative quantities at Σ .

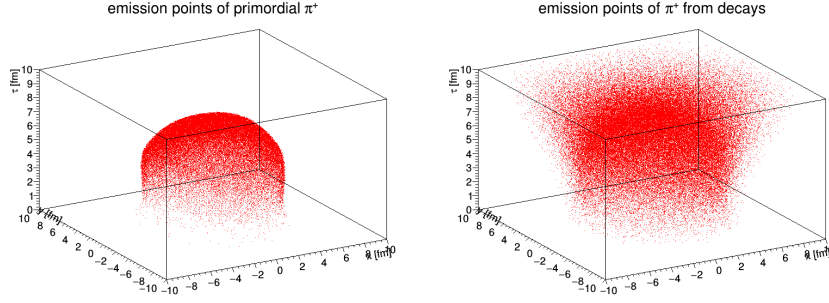


Fig. 8 Emission points of primordial π^+ (left panel), and π^+ from decays (right panel) in the $x-y-\tau$ plane in Au-Au collisions at $\sqrt{s_{NN}} = 200$ GeV and the impact parameter of 7.16 fm.

$$P(N_k) = \frac{(\bar{N}_k)^{N_k}}{N_k!} \exp(-\bar{N}_k) \quad (59)$$

For each particle species k number N_k of particles is generated according to the von-Neumann acceptance/rejection procedure: space-time point (ζ, ϕ, θ) at Σ , momentum components of the particle $(p_T, \phi_p$ and $y_p)$, and a test variable $\mathcal{F}_{\text{test}}^k$ in the range $\langle 0, \mathcal{F}_{\text{max}}^k \rangle$, are generated randomly. The particle is accepted if $\mathcal{F}_{\text{test}}^k < \mathcal{F}^k(\zeta, \phi, \theta, p_T, \phi_p, y_p)$, otherwise it is rejected. The generation of particles goes over all species (stable ones and resonances), which are listed in the Particle Data Group [59] tables, and whose properties are known well enough. For that purpose the SHARE particle database is used [66].

- Once the ensemble of primordial particles is generated the code performs decays of unstable resonances, which, in general, may proceed in cascades. Each resonance evolves along the classical trajectory starting from its initial position x_{origin}^μ according to its momentum

$$x_{\text{decay}}^\mu = x_{\text{origin}}^\mu + \frac{p^\mu}{m_k} \Delta \tau. \quad (60)$$

and decays after its lifetime $\Delta \tau$, which is randomly generated with the probability density $\Gamma_k \exp(-\Gamma_k \Delta \tau)$, where Γ_k is the width of the particle of species k . The particular decay channel is selected randomly with the probability corresponding to its branching ratio. The decays of sub-threshold type are not allowed. The decays, which are of two-particle or three-particle type, follow simple kinematic formulas [63], and are treated on equal footing. All required data on the decays follows from the SHARE particle decays database [66].

- Once all particles in the event decayed, the calculation is completed.

The exemplar emission points in space-time obtained with the initial tilted source and THERMINATOR simulations are presented in the Fig. 8. In the next Section, based on the data on the emitted particles, we will calculate some physical observables.

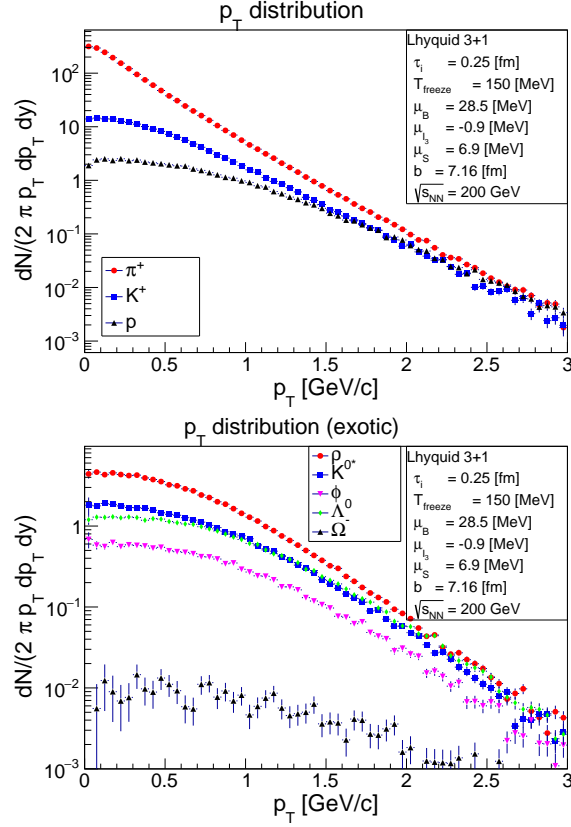


Fig. 9 Transverse-momentum spectra of π^+ , K^+ , and protons (top panel) and ρ mesons, K_0^* mesons, ϕ mesons, Λ^0 baryons, and Ω^- baryons (bottom panel) for Au-Au collisions at $\sqrt{s_{\text{NN}}} = 200$ GeV and the impact parameter of 7.16 fm (protons from the weak decays of Λ 's are excluded). The statistics of 3000 events was used. The errors are statistical only.

13 Performing analysis with THERMINATOR2

Due to the detailed record on properties of all produced particles, including their space-time coordinates (x^μ, p^μ) and their decay chains, the THERMINATOR code becomes a versatile tool, allowing for calculation of various observables. Having completed generation of events various experimental observables may be calculated, either, by using the figure macros supplied with the code, or, by preparing user macros. In this Section we will present some of its capabilities.

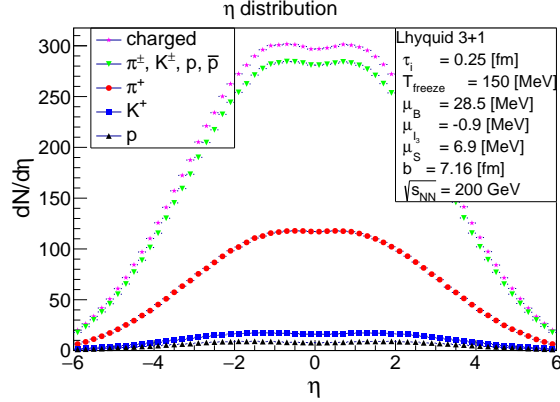


Fig. 10 Pseudorapidity spectra of π^+ , K^+ , and protons shown separately, and summed together with their antiparticles, as well as of all charged particles, for Au-Au collisions at $\sqrt{s_{\text{NN}}} = 200$ GeV and the impact parameter of 7.16 fm. The statistics of 3000 events was used. The errors are statistical only.

13.1 Single-particle spectra

One of the most straightforward observables to calculate is the single-particle spectrum of certain particle species k . The most copiously produced ones are the lightest mesons (pions and kaons) and baryons (protons). They form more than 90% of the total charged particles. In the Fig. 9 we present the transverse-momentum spectra of π^+ , K^+ , and protons (top panel), as well as ρ mesons, K_0^* mesons, ϕ mesons, Λ^0 baryons, and Ω^- baryons (bottom panel) for Au-Au collisions at $\sqrt{s_{\text{NN}}} = 200$ GeV and the impact parameter of 7.16 fm. All results were obtained using the fluid dynamical input, obtained with event-averaged “tilted” initial conditions and the freeze-out temperature $T_{\text{freeze}} = 150$ MeV. The chemical potentials $\mu_B = 28.5$ MeV, $\mu_{I_3} = -0.9$ MeV, and $\mu_S = 6.9$ MeV were included at the freeze-out solely. The presentation of results is limited to the “soft” transverse momenta ($p_T < 3$ GeV), where the fluid dynamical models are expected to be applicable, and the midrapidity region, $|y_p| < 1$. One observes that slopes of the spectra are species-dependent, which is mainly due to their different masses. At intermediate momenta the spectra have exponential shapes, which is characteristic for thermal systems. At low p_T various effects play role, see next section. In the Fig. 10 we present the respective p_T -integrated pseudorapidity distribution of charged particles, where $\eta = \ln[(p + p_z)/(p - p_z)]/2$. The latter are compared to the contributions from π^+ , K^+ , and protons. One observes that, while the central rapidity region $y_p \approx \eta$ is approximately boost-invariant, the forward/backward rapidity regions are not. This is a result of using full four-dimensional fluid dynamical simulations of the emitting source.

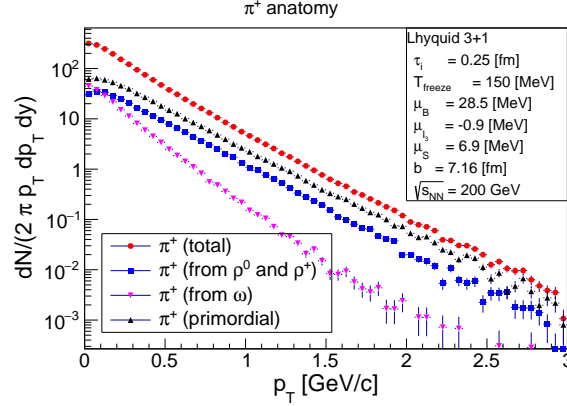


Fig. 11 The anatomy of the transverse-momentum spectra of π^+ for Au-Au collisions at $\sqrt{s_{NN}} = 200$ GeV, and the impact parameter of 7.16 fm. The spectrum of primordial pions, as well as the contribution from ρ^0 , ρ^+ and ω resonance decays, is presented. The statistics of 3000 events was used. The errors are statistical only.

13.2 Impact of resonance decays

One of the effects which significantly affects shapes of the single-particle spectra are decays of resonances. Due to available phase space they populate mainly the low- p_T region of the spectra. In the Fig. 11 we present the “anatomy” of the transverse-momentum spectra of π^+ . One observes that the low- p_T part of the spectrum of primordial pions (produced directly at the freeze-out hypersurface) and the total spectrum (including the contribution from all resonance decays) differ significantly. The primordial pions develop a characteristic knee in the soft region. The decays of heavy resonances feed up the spectrum in this region, see contribution from ω decays in the Fig. 11. As a result the total shape of pion spectrum takes the characteristic concave shape. Moreover, the effective slope of the final spectrum becomes steeper which manifests itself by the lower effective temperature of the spectrum, see Sec. 10.

13.3 Experimental feed-down corrections

The experimental proton spectra are usually feed-down corrected for $\Lambda^0 \rightarrow p^+ + \pi^-$ weak decays. Such corrections are straightforward to be included in THERMINATOR analysis, and they were also applied in Fig. 9. In the Fig. 12 we present the comparison of proton spectra with and without applying these corrections. We observe that the feed-down from weak-decays is at the level of 30%, which is a significant correction.

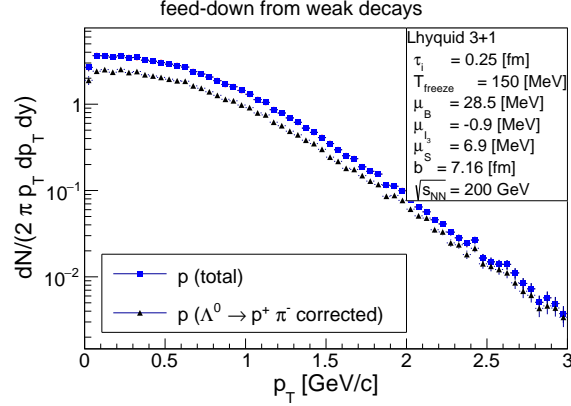


Fig. 12 Transverse-momentum spectra of protons, with, and without feed-down correction for $\Lambda^0 \rightarrow p^+ + \pi^-$ weak decays. The statistics of 3000 events was used. The errors are statistical only.

T_{freeze} [MeV]	130	150	170
K^+/π^+	0.199	0.263	0.326
p/π^+	0.033	0.065	0.110

Table 1 The K^+/π^+ and p/π^+ total yield ratios calculated at various freeze-out temperatures $T_{\text{freeze}} \in \{130, 150, 170\}$ MeV.

13.4 Ratios of particle yields

As it was discussed in Sec. 10 the inclusion of resonance decays was crucial for the proper description of the ratios of particle yields, giving the chemical freeze-out temperatures of the order of the critical temperature of the phase-transition in QCD. Following some recent studies, which focus on reproducing the shapes of the spectra rather than the yields ratios, the freeze-out temperatures extracted from the data can be as low as 150 MeV (sometimes even lower). One should expect that, in such a case, one should observe a decrease of quality of the fits of the particle abundances. To see this, in Table 1 we present the K^+/π^+ and p/π^+ total yield ratios calculated at various freeze-out temperatures T_{freeze} . One observes that with reducing the freeze-out temperature the ratios decrease which is consequence of the fact that heavy particles are most copiously produced at large temperatures. The decrease is more significant for protons than for kaons. The results suggest that the fitting of particle spectra should be always accompanied by the fits of particle yields.

Acknowledgements The author would like to express his gratitude to the Organizers of the 53rd Karpacz Winter School of Theoretical Physics and THOR COST Action Training School for their help and hospitality. This work was supported by the THOR COST Action CA15213, ExtreMe Matter Institute EMMI at the GSI Helmholtzzentrum für Schwerionenforschung, Darmstadt, Germany, and the Polish National Science Center grants No. DEC-2012/07/D/ST2/02125 and DEC-2016/23/B/ST2/00717.

References

- [1] Li Yan. A flow paradigm in heavy-ion collisions. 2017.
- [2] Wojciech Florkowski and Radoslaw Ryblewski. Highly-anisotropic and strongly-dissipative hydrodynamics for early stages of relativistic heavy-ion collisions. *Phys. Rev.*, C83:034907, 2011.
- [3] Mauricio Martinez and Michael Strickland. Dissipative Dynamics of Highly Anisotropic Systems. *Nucl. Phys.*, A848:183–197, 2010.
- [4] Mubarak Alqahtani, Mohammad Nopoush, Radoslaw Ryblewski, and Michael Strickland. 3+1d quasiparticle anisotropic hydrodynamics for ultrarelativistic heavy-ion collisions. *Phys. Rev. Lett.*, 119(4):042301, 2017.
- [5] Michael Strickland. Anisotropic Hydrodynamics: Three lectures. *Acta Phys. Polon.*, B45(12):2355–2394, 2014.
- [6] Mubarak Alqahtani, Mohammad Nopoush, and Michael Strickland. Relativistic anisotropic hydrodynamics. 2017.
- [7] Wojciech Florkowski, Radoslaw Ryblewski, and Michael Strickland. Testing viscous and anisotropic hydrodynamics in an exactly solvable case. *Phys. Rev.*, C88:024903, 2013.
- [8] Wojciech Florkowski, Radoslaw Ryblewski, and Michael Strickland. Anisotropic Hydrodynamics for Rapidly Expanding Systems. *Nucl. Phys.*, A916:249–259, 2013.
- [9] Gabriel S. Denicol, Ulrich W. Heinz, Mauricio Martinez, Jorge Noronha, and Michael Strickland. New Exact Solution of the Relativistic Boltzmann Equation and its Hydrodynamic Limit. *Phys. Rev. Lett.*, 113(20):202301, 2014.
- [10] Gabriel S. Denicol, Ulrich W. Heinz, Mauricio Martinez, Jorge Noronha, and Michael Strickland. Studying the validity of relativistic hydrodynamics with a new exact solution of the Boltzmann equation. *Phys. Rev.*, D90(12):125026, 2014.
- [11] Wojciech Florkowski, Michal P. Heller, and Michal Spalinski. New theories of relativistic hydrodynamics in the LHC era. 2017.
- [12] Amaresh Jaiswal, Radoslaw Ryblewski, and Michael Strickland. Transport coefficients for bulk viscous evolution in the relaxation time approximation. *Phys. Rev.*, C90(4):044908, 2014.
- [13] Wojciech Florkowski, Amaresh Jaiswal, Ewa Maksymiuk, Radoslaw Ryblewski, and Michael Strickland. Relativistic quantum transport coefficients for second-order viscous hydrodynamics. *Phys. Rev.*, C91:054907, 2015.

- [14] Leonardo Tinti, Amaresh Jaiswal, and Radoslaw Ryblewski. Quasiparticle second-order viscous hydrodynamics from kinetic theory. *Phys. Rev.*, D95(5):054007, 2017.
- [15] Wojciech Florkowski, Radoslaw Ryblewski, Michael Strickland, and Leonardo Tinti. Non-boost-invariant dissipative hydrodynamics. *Phys. Rev.*, C94(6):064903, 2016.
- [16] L.D. Landau and E.M. Lifshitz. *Fluid Mechanics*. 1959.
- [17] Charles W. Misner, K. S. Thorne, and J. A. Wheeler. *Gravitation*. W. H. Freeman, San Francisco, 1973.
- [18] S.R. de Groot, W.A. van Leeuwen, and Ch.G. van Weert. *Relativistic Kinetic Theory: Principles and Applications*. 1980.
- [19] L. Rezzolla and O. Zanotti. *Relativistic Hydrodynamics*. OUP Oxford, 2013.
- [20] Horst Stoecker and W. Greiner. High-Energy Heavy Ion Collisions: Probing the Equation of State of Highly Excited Hadronic Matter. *Phys. Rept.*, 137:277–392, 1986.
- [21] Dirk H. Rischke. *Fluid dynamics for relativistic nuclear collisions*, pages 21–70. Springer Berlin Heidelberg, Berlin, Heidelberg, 1999.
- [22] Peter F. Kolb and Ulrich W. Heinz. Hydrodynamic description of ultrarelativistic heavy ion collisions. 2003.
- [23] P. Huovinen and P. V. Ruuskanen. Hydrodynamic Models for Heavy Ion Collisions. *Ann. Rev. Nucl. Part. Sci.*, 56:163–206, 2006.
- [24] Wojciech Florkowski. *Phenomenology of Ultra-Relativistic Heavy-Ion Collisions*. 2010.
- [25] Paul Romatschke. New Developments in Relativistic Viscous Hydrodynamics. *Int. J. Mod. Phys.*, E19:1–53, 2010.
- [26] Charles Gale, Sangyong Jeon, and Bjoern Schenke. Hydrodynamic Modeling of Heavy-Ion Collisions. *Int. J. Mod. Phys.*, A28:1340011, 2013.
- [27] Amaresh Jaiswal and Victor Roy. Relativistic hydrodynamics in heavy-ion collisions: general aspects and recent developments. *Adv. High Energy Phys.*, 2016:9623034, 2016.
- [28] Mikolaj Chojnacki and Wojciech Florkowski. Temperature dependence of sound velocity and hydrodynamics of ultra-relativistic heavy-ion collisions. *Acta Phys. Polon.*, B38:3249–3262, 2007.
- [29] J. D. Bjorken. Highly Relativistic Nucleus-Nucleus Collisions: The Central Rapidity Region. *Phys. Rev.*, D27:140–151, 1983.
- [30] Steven S. Gubser. Symmetry constraints on generalizations of Bjorken flow. *Phys. Rev.*, D82:085027, 2010.
- [31] G. S. Denicol. Kinetic foundations of relativistic dissipative fluid dynamics. *J. Phys.*, G41(12):124004, 2014.
- [32] Piotr Bozek and Iwona Wyskiel. Directed flow in ultrarelativistic heavy-ion collisions. *Phys. Rev.*, C81:054902, 2010.
- [33] Michael L. Miller, Klaus Reygers, Stephen J. Sanders, and Peter Steinberg. Glauber modeling in high energy nuclear collisions. *Ann. Rev. Nucl. Part. Sci.*, 57:205–243, 2007.

- [34] J. P. Bondorf, S. I. A. Garpman, and J. Zimanyi. A Simple Analytic Hydrodynamic Model for Expanding Fireballs. *Nucl. Phys.*, A296:320–332, 1978.
- [35] Ulrich W. Heinz and Gregory Kestin. Jozso’s Legacy: Chemical and Kinetic Freeze-out in Heavy-Ion Collisions. *Eur. Phys. J. ST*, 155:75–87, 2008.
- [36] Wojciech Broniowski and Wojciech Florkowski. Explanation of the RHIC $p(T)$ spectra in a thermal model with expansion. *Phys. Rev. Lett.*, 87:272302, 2001.
- [37] Wojciech Broniowski and Wojciech Florkowski. Strange particle production at RHIC in a single freezeout model. *Phys. Rev.*, C65:064905, 2002.
- [38] Wojciech Broniowski, Anna Baran, and Wojciech Florkowski. Thermal approach to RHIC. *Acta Phys. Polon.*, B33:4235–4258, 2002.
- [39] Wojciech Broniowski, Anna Baran, and Wojciech Florkowski. Thermal model at RHIC. Part 2. Elliptic flow and HBT radii. *AIP Conf. Proc.*, 660:185–195, 2003. [,185(2002)].
- [40] Piotr Bozek, Wojciech Broniowski, and Wojciech Florkowski. Balance functions in a thermal model with resonances. *Acta Phys. Hung.*, A22:149–157, 2005.
- [41] Wojciech Broniowski, Wojciech Florkowski, and Brigitte Hiller. Thermal analysis of production of resonances in relativistic heavy ion collisions. *Phys. Rev.*, C68:034911, 2003.
- [42] Adam Kisiel, Wojciech Florkowski, and Wojciech Broniowski. Femtoscopy in hydro-inspired models with resonances. *Phys. Rev.*, C73:064902, 2006.
- [43] Pasi Huovinen and Hannah Petersen. Particlization in hybrid models. *Eur. Phys. J.*, A48:171, 2012.
- [44] Piotr Bozek and Iwona Wyskiel. Rapid hydrodynamic expansion in relativistic heavy-ion collisions. *Phys. Rev.*, C79:044916, 2009.
- [45] Radoslaw Ryblewski. Anisotropic hydrodynamics for ultra-relativistic heavy-ion collisions. *J. Phys.*, G40:093101, 2013.
- [46] Fred Cooper and Graham Frye. Comment on the Single Particle Distribution in the Hydrodynamic and Statistical Thermodynamic Models of Multiparticle Production. *Phys. Rev.*, D10:186, 1974.
- [47] Mikolaj Chojnacki, Wojciech Florkowski, Wojciech Broniowski, and Adam Kisiel. Soft heavy-ion physics from hydrodynamics with statistical hadronization: Predictions for collisions at $S^{*(1/2)}(NN) = 5.5$ -TeV. *Phys. Rev.*, C78:014905, 2008.
- [48] Mikolaj Chojnacki, Adam Kisiel, Wojciech Florkowski, and Wojciech Broniowski. THERMINATOR 2: THERMal heavy IoN generATOR 2. *Comput. Phys. Commun.*, 183:746–773, 2012.
- [49] Ulrich W. Heinz. Strange messages: Chemical and thermal freezeout in nuclear collisions. *J. Phys.*, G25:263–274, 1999.
- [50] Jean Cleymans, Helmut Oeschler, and Krzysztof Redlich. Particle ratios at SPS, AGS and SIS. *J. Phys.*, G25:281–285, 1999.
- [51] P. Braun-Munzinger, D. Magestro, K. Redlich, and J. Stachel. Hadron production in Au - Au collisions at RHIC. *Phys. Lett.*, B518:41–46, 2001.

- [52] Wojciech Florkowski, Wojciech Broniowski, and Mariusz Michalec. Thermal analysis of particle ratios and $p(t)$ spectra at RHIC. *Acta Phys. Polon.*, B33:761–769, 2002.
- [53] Johann Rafelski, Jean Letessier, and Giorgio Torrieri. Strange hadrons and their resonances: A Diagnostic tool of QGP freezeout dynamics. *Phys. Rev.*, C64:054907, 2001. [Erratum: *Phys. Rev.*C65,069902(2002)].
- [54] Anna Baran, Wojciech Broniowski, and Wojciech Florkowski. Description of the particle ratios and transverse momentum spectra for various centralities at RHIC in a single freezeout model. *Acta Phys. Polon.*, B35:779–798, 2004.
- [55] Ludwik Turko. Statistical models of hadron production: Simple models for complicated processes. *Phys. Part. Nucl.*, 39:1095–1101, 2008.
- [56] P. Braun-Munzinger, J. Stachel, and Christof Wetterich. Chemical freezeout and the QCD phase transition temperature. *Phys. Lett.*, B596:61–69, 2004.
- [57] Szabolcs Borsanyi, Gergely Endrodi, Zoltan Fodor, Antal Jakovac, Sandor D. Katz, Stefan Krieg, Claudia Ratti, and Kalman K. Szabo. The QCD equation of state with dynamical quarks. *JHEP*, 11:077, 2010.
- [58] R. Hagedorn. Statistical thermodynamics of strong interactions at high-energies. *Nuovo Cim. Suppl.*, 3:147–186, 1965.
- [59] Claude Amsler et al. Review of Particle Physics. *Phys. Lett.*, B667:1–1340, 2008.
- [60] Ekkard Schnedermann, Josef Sollfrank, and Ulrich W. Heinz. Thermal phenomenology of hadrons from 200-A/GeV S+S collisions. *Phys. Rev.*, C48:2462–2475, 1993.
- [61] Mikolaj Chojnacki, Wojciech Florkowski, and Tamas Csorgo. On the formation of Hubble flow in little bangs. *Phys. Rev.*, C71:044902, 2005.
- [62] Viktor Begun, Wojciech Florkowski, and Maciej Rybczynski. Explanation of hadron transverse-momentum spectra in heavy-ion collisions at $\sqrt{s_{NN}} = 2.76$ TeV within chemical non-equilibrium statistical hadronization model. *Phys. Rev.*, C90(1):014906, 2014.
- [63] Adam Kisiel, Tomasz Taluc, Wojciech Broniowski, and Wojciech Florkowski. THERMINATOR: THERMal heavy-IoN generATOR. *Comput. Phys. Commun.*, 174:669–687, 2006.
- [64] R. Brun and F. Rademakers. ROOT: An object oriented data analysis framework. *Nucl. Instrum. Meth.*, A389:81–86, 1997.
- [65] THERMINATOR2 project website. <https://therminator2.ifj.edu.pl/>. Generated on Sun Jul 17 2011 20:57:54.
- [66] Giorgio Torrieri, S. Steinke, Wojciech Broniowski, Wojciech Florkowski, Jean Letessier, and Johann Rafelski. SHARE: Statistical hadronization with resonances. *Comput. Phys. Commun.*, 167:229–251, 2005.